BIO BRAGG GRATINGS ON MICROFIBERS FOR LABEL-FREE BIOSENSING

Augusto Juste-Dolz[1], Martina Delgado-Pinar[2], Miquel Avella-Oliver[1,4,*], Estrella Fernández[1], Daniel Pastor[3], Miguel V. Andrés[2], Ángel Maquieira[1,4,**]

[1] Instituto Interuniversitario de Investigación de Reconocimiento Molecular y Desarrollo Tecnológico (IDM), Universitat Politècnica de València, Universitat de València, 46022 Valencia, Spain.

[2] Department of Applied Physics and Electromagnetism-ICMUV, Universitat de València, Burjassot 46100, Spain.

[3] Photonics Research Labs, Universitat Politècnica de València, 46021 Valencia, Spain.

[4] Departamento de Química, Universitat Politècnica de València, 46022 Valencia, Spain.

** Corresponding author.*

*** Corresponding author.*

E-mail addresses: miavol@upv.es (M. Avella-Oliver), amaquieira@qim.upv.es (Á. Maquieira).

Abstract: Discovering nanoscale phenomena to sense biorecognition events introduces new perspectives to exploit nanoscience and nanotechnology for bioanalytical purposes. Here we present Bio Bragg Gratings (BBGs), a novel biosensing approach that consists of diffractive structures of protein bioreceptors patterned on the surface of optical waveguides, and tailored to transduce the magnitude of biorecognition assays into the intensity of single peaks in the reflection spectrum. This work addresses the design, fabrication, and optimization of this system by both theoretical and experimental studies to explore the fundamental physicochemical parameters involved. Functional biomolecular gratings are fabricated by

microcontact printing on the surface of tapered optical microfibers, and their structural features were characterized. The transduction principle is experimentally demonstrated, and its quantitative bioanalytical prospects are assessed in a representative immunoassay, based on patterned protein probes and selective IgG targets, in label-free conditions. This biosensing system involves appealing perspectives to avoid unwanted signal contributions from non-specific binding, herein investigated in human serum samples. The work also proves how the optical response of the system can be easily tuned, and it provides insights into the relevance of this feature to conceive multiplexed BBG systems capable to perform multiple label-free biorecognition assays in a single device.

Keywords: biosensor, diffraction, optical microfiber, immunoassay, non-specific binding, label-free

1. INTRODUCTION

The advances in chemistry, biotechnology and nanoscience have introduced exciting strategies to sense biomacromolecules (Mahmoudpour et al., 2019; Xu et al., 2020; Zhang et al., 2020) and the interaction events between them (Bhattacharyya et al., 2019; Escorihuela et al., 2015; Schneider and Niemeyer, 2018). Discovering new nanoscale phenomena to transduce biorecognition processes into measurable signals open new potential venues to materialize the benefits that nanoscience offers in key areas of today's society, such as medicine and pharmacology (Prasad et al., 2019; Wong et al., 2020; Zhang et al., 2020).

The implementation of some optical phenomena for biosensing such as SPR (Nootchanat et al., 2019; Zhao et al., 2019), SERS (Langer et al., 2020; Liu et al., 2020), and light interference (Chen et al., 2019; J. Wang et al., 2020) became the seed of a high scientific activity in the last decades, which have provided a great knowledge on innovative, sensitive and label-free bioanalytical systems. Along these lines, light

diffraction is still a promising and rather unexplored phenomena to transduce biorecognition events, as introduced by some investigations focused on diffraction-based sensing (Avella-Oliver et al., 2017, 2018; Goh et al., 2002, 2005) and focal molography (Frutiger et al., 2020, 2019; Gatterdam et al., 2017).

On the other hand, the integration of transduction principles in optical fibers presents a great potential to conceive miniaturized, inexpensive, low-loss, and compact systems for in-field analysis. This approach constitutes nowadays an important innovation area in the state-of-the-art, for both (bio)chemical and physical sensing (Wang and Wolfbeis, 2020; Zhao et al., 2020). A paradigmatic strategy in this context is to inscribe a periodic modulation in the refractive index of the core material of optical fibers or microfibers, thus fabricating special fiber Bragg gratings (FBGs), microfiber Bragg gratings, long period gratings, and tilted fiber Bragg gratings whose optical response is designed to be sensitive to the presence of analytes in the external medium surrounding the optical device (Bekmurzayeva et al., 2018; Cao et al., 2017, Delgado-Pinar et al., 2017; Liu et al., 2018; Loyez et al., 2020; Malachovská et al., 2015; Sridevi et al., 2015; Sypabekova et al., 2019).

In this study, we present a novel transduction principle to sense biorecognition events based on periodic networks of bioreceptors patterned on the surface of tapered optical fibers, herein called Bio Bragg Gratings (BBGs). As schematized in Fig. 1, the concept behind this idea relies on using a microfiber, whose optical modes present a significant evanescent field in the external medium, and imprinting a periodic biomolecular network along its surface. The fundamental optical mode will interact with the BBG, and it will result on a reflection peak centered at the optical wavelength that fulfills the Bragg condition. The biosensing transduction principle relies on the fact that binding events between the patterned bioreceptors and their targets in solution modify the amount of matter constituting the strips of the BBG (compared to the gaps), thus the presence of the analyte will change the modulation depth of the BBG. Consequently, this system aims to transduce the magnitude of binding

events by means of the peak reflectivity. In addition to the novelty, this strategy projects potential prospects for label-free biosensing, with simple and inexpensive materials, and neglecting signal contributions generated by non-specific bindings (Gatterdam et al., 2017).

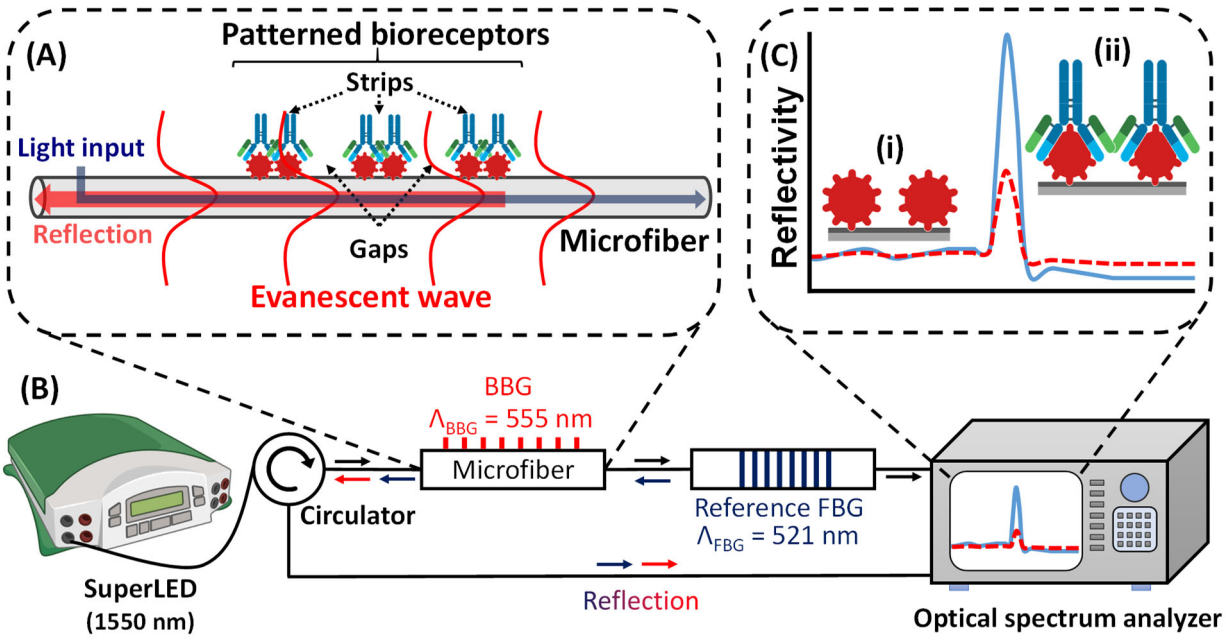

Fig. 1. General illustration of the approach. (A) Scheme of a BBG on a microfiber, and its interaction with the guided light. (B) Scheme of the detection setup. See Fig. S1 for real images and additional setup details. (C) Optical response in the reflection spectrum before (i, and red dashed line) and after (ii, and blue continuous line) incubation and binding of target compounds on the patterned bioreceptors of the BBG.

Herein we present the design, fabrication, and optimization of the BBGs in tapered microfibers, and report our investigations to explore and prove the concept of this biosensing transduction system. This work addresses an optical and functional characterization of the system by both theoretical and experimental studies using a model immunochemical assay. A custom setup is developed to fabricate the BBGs on tapered microfibers, and the structural features of the resulting bioreceptor networks are characterized by electron microscopy. Finally, this study demonstrates the bioanalytical performance of the system, provide insights into prospective biosensing properties of BBGs and discusses them.

2. MATERIALS AND METHODS

2.1 Materials

Sodium phosphate buffer (PBS, 8 mM Na_2HPO_4, 2 mM, 137 mM NaCl, 2.7 mM KCl, pH 7.4), PBS-T (PBS with polysorbate 20 0.05% v/v), were prepared with purified water (Milli-Q, Millipore Iberica, Darmstadt, Germany) and filtered through 0.2 µm polyethersulfone membranes (Merck, Darmstadt, Germany). Polydimethylsiloxane (PDMS) Sylgard 184 was from Dow Corning (Wiesbaden, Germany). Bovine serum albumin (BSA), polysorbate 20 (Tween 20), antiBSA rabbit IgG, C-reactive protein (CRP), casein and human serum (human male, AB plasma) were supplied by Sigma-Aldrich (Madrid, Spain). Single-mode optical fibers SMF-28 were purchased from Corning (Madrid, Spain). The silicon grooved nanostructure (555.5 nm period, 140 nm groove depth, duty cycle 50%) used as a master to prepare the micro-contact printing stamp, was from LightSmyth (Eugene, OR, USA).

2.2 Simulations

Electromagnetic simulations to calculate the optical response of the system were carried out by means of finite difference method in the Quasi TE & TM approach, implemented on Matlab™ (Rumpf et al., 2014; Zhu and Brown, 2002). Electromagnetic fields distribution results were validated with commercial software MODE Lumerical (Finite Difference Eigenmode). The overlapping integrals (i.e. proportion of the total field interacting with the Bragg perturbation) were calculated from the obtained field distribution over the complete waveguide and compared with the field localized onto the BBG area. Then, the contradirectional coupling coefficient and the device reflectivity were calculated with the well-known closed form expressions for periodically perturbed waveguides (Erdogan, 1997; Yariv and Yeh, 2007).

An incident wavelength of 1550 nm and refractive indexes of 1.43 for biomolecules (Freeman et al., 2004; Sancho-Fornes et al., 2019) and 1.446 for silica microfibers

were considered. For the simulations, the BBGs were defined as 2 mm long periodic (period = 555nm, duty cycle = 50 %) gratings of biomolecules that cover a 90° section of the total azimuthal coordinate of the fiber surface. The thickness of the printed strips in the simulations was considered 1 nm for BSA BBGs (i.e., before target incubation) and 10 nm for BSA-IgG BBGs (i.e., after target incubation) (Avella-Oliver et al., 2018).

2.3 Microfibers

Microfibers were fabricated by tapering standard single mode fibers (Corning SMF-28, 125 μm of diameter) by means of the pull-and-fuse technique. This process consists on the controlled pulling of a conventional fiber, while it is heated up to the plastic deformation temperature of the silica (Fig. S2). As described elsewhere (Birks and Li, 1992), this system allows to obtain uniform microfibers of several centimeters long, with diameters of the waist down to 1 μm. After fabrication, microfibers were fixed in a custom holder that keep them taut (Fig. S3).

2.4 BBG patterning

Nanostructured networks of bioreceptors (BBGs), constituted by periodic parallel strips of biomacromolecules and empty gaps between them (Fig. 1A), were patterned onto the surface of microfibers by microcontact printing and immobilized. For that, PDMS (elastomer:curing agent, 10:1 w/w) was poured onto the nanogrooved side of the silicon master, degassed in a vacuum chamber for 5 min, and polymerized overnight at 60 °C. Then, the cured polymer was peeled off from the master and cut in 10 × 5 mm pieces, and these stamps were washed three times by sonication in ethanol (30% in water, 5 min) and dried under a stream of air. Probe solutions in PBS (80 μL, 250 μg mL^{-1}) were incubated on the structured side of the stamps and after 160 min they were rinsed with deionized water and dried by air stream, thus obtaining BBGs of physisorbed probes on the fiber (Juste-Dolz et al., 2018).

A custom setup was created to pattern the BBGs onto tapered fibers, based on a mechanical elevator that uplifts the inked stamps until their grooved side becomes in

contact with the microfiber. A detailed description on the configuration and use of this setup is reported in Fig. S4. The optical response of the system was measured with the detection setup described below and used to monitor the stamping processes (Fig. S5).

The topography of the resulting BBGs was analysed by Field Emission Scanning Electron Microscopy (FESEM), using a ZEISS ULTRA-55 scanning electron microscope (ZEISS, Oxford Instruments).

2.5 Biorecognition assays

First, to perform and quantify the immunoassays, once fabricated the probe BBGs their optical responses were measured in air (as described in sections 2.6 and 2.7 below). Then, the microfibers containing the BBGs were immersed in 600 µL of liquid samples and incubated for 30 min. A custom incubation chamber made of PDMS was used to keep the fiber immersed within the liquid samples during the incubations. Subsequently, the fibers were rinsed with PBS-T and deionized water, and dried in air. Finally, the optical response of the BBGs after the biorecognition were measured in air. All the measurements and incubations were performed at room temperature.

2.6 Optical setup

The scheme of the optical setup is shown in Fig. 1B. The optical light was provided by an infrared LED source (1.3 mW continuous wave, central wavelength: 1550nm, bandwidth > 100 nm), and it was launched to the microfiber through an optical circulator (Thorlabs, operation wavelength: 1550nm, bandwidth: 90nm). Thus, both transmission and reflection spectra were measured. An optical spectrum analyser AQ6370D, Yokogawa, 600 -1700 nm, minimum resolution 20 pm, was used to acquire the spectra. An additional FBG, written using UV radiation in the core of commercial photosensitive fiber (Fibercore PS1250) by means of the phase-mask technique, was included in the setup (Fig. S6). The peak intensity of this grating serves as a reference to monitor and correct potential power level changes introduced in the fabrication

process and the immunoassays, as well as power level fluctuations (Supplementary Information 7).

2.7 Data acquisition and processing

Transmission and reflection spectra were acquired in each step of the BBGs fabrication and the subsequent biosensing assays. The data was analyzed in both logarithmic and linear scale, and a detailed description of this processing is provided in the Supplementary Information 10. All optical traces were registered within the range 1500-1580 nm with a spectral resolution of 50 pm, and the variation in the peak reflectivity was used as the analytical signal. This net reflectivity was calculated as the difference between the peak reflectivity registered after patterning the probes, and after incubating the targets, as detailed in the Supplementary Information 7 and Fig. S8.

Noise was estimated as the standard deviation from 10 blank measurements (0 μg mL^{-1} of target IgG incubated on BBGs fabricated on 10 different fibers) that we employed to infer signal-to-noise ratios (SNR). Limits of detection and quantification were calculated from experimental dose-response curves as the concentrations associated to SNR = 3 and SNR = 10, respectively.

3. RESULTS AND DISCUSSION

3.1 Microfibers design

The diameter of the microfiber is a key parameter in this BBG concept, since it determines the fraction of light in the evanescent field of the optical mode. It will ultimately affect the magnitude of the diffractive interaction with the bioreceptors and define the performance of resulting the biosensing transduction. Hence, theoretical calculations were performed beforehand experimental assessments to set the starting working conditions.

Firstly, the overlap integral between the fundamental optical mode (LP_{01}) and the diffractive nanostructure of bioreceptors (BBG) on the microfiber was calculated as a

function of the diameter of the microfiber. As shown in Fig. 2A, as the diameter increases, the stronger confinement of the mode within the microfiber leads to a negligible overlap integral. However, when the microfiber diameter becomes comparable to the light wavelength, the evanescent field enlarges and the fraction of light overlapping the BBG displays an exponential growth. These preliminary insights are also supported by the calculations of the corresponding peak reflectivity of such BBGs (Fig. 2B), where the reflectivity increases (together with the overlap integral) when the fiber diameter decreases.

The BBG is located at one side of the fiber, which leads to an anisotropic system whose optical response must be dependent on the orientation of the linear polarization of the optical mode, partly due to the different position of the evanescent tail of the mode for each polarization (see Fig. 2C). Therefore, to perform a rigorous analysis, the optical response in both linear polarizations (X and Y) were also calculated together with the overlap integral and the peak reflectivity. As observed in Fig. 2A and 2B, for a 3 μm diameter there is difference of around 3dB in the peak intensity between the two polarizations, which corresponds to a reduction in the fields overlapping of about a 50% and highlights the role of the polarization in this system. However, the anisotropic behavior of the BBG was not observed in the subsequent experimental immunoassays (section 3.3).

From these results and considering the manipulation feasibility of microfibers below 1 μm, fiber diameters from 2 to 5 microns were selected to experimentally investigate the BBG concept.

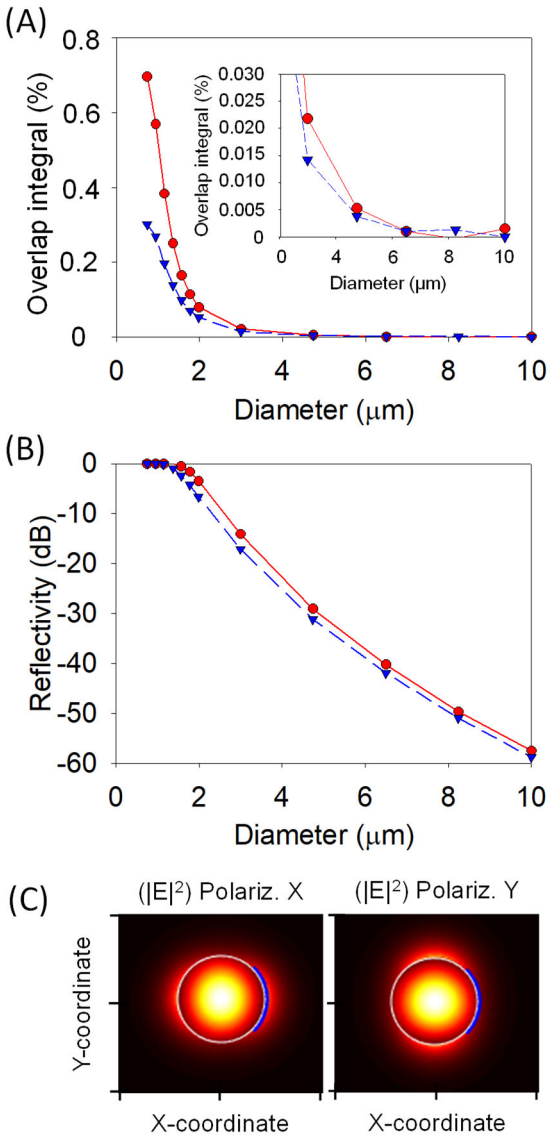

Fig. 2. Simulated optical response for different microfiber diameters. (A) Overlap integral and (B) reflectivity for the fundamental optical mode, a BBG thickness of 10 nm, and at both orientations of the linear polarization of the optical mode (red continuous line for X polarization and blue dashed line for Y polarization). The inset in Figure 2A zooms in the overlap integral at larger diameters for a better visualization. (C) Electric field intensity distribution for both polarizations in a 1 μm microfiber. The blue line at the right side of both plots, represents the microfiber section covered by the BBG.

3.2 Structural and functional characterization of the BBGs.

A critical step in this approach is the BBG patterning, and herein we address it by microcontact printing. This is an important and versatile technique in the state-of-art (Lamping et al., 2019; X. Wang et al., 2020), widely used to create functional and

homogeneous patterns of biomolecules onto flat substrates of different compositions (Juste-Dolz et al., 2018). However, it remains challenging to pattern biomacromolecules onto curved, fragile, and micrometric structures as microfibers. In this work we successfully addressed this issue with a half-assisted setup that allows a practical manipulation of the microfibers and monitors the transmission spectrum of the optical device as a feedback system to control the nanoscopic patterning process taking place on the fiber surface. For this assessment, we patterned BBGs of physisorbed bovine serum albumin (BSA) probes on 5 μm microfibers.

As can be seen in Fig. 3, homogeneous periodic grooved structures are generated onto the surface of the microfiber, where darker vertical lines are the protein strips of the BBG, and the greyish ones are the gaps between them. A grating period (Λ_{BBG}) of 556 ± 1 nm was calculated from FESEM images (Fig. 3B), which agrees with the period of the original master structure (555 nm). However, as protein strips are thinner than the gaps the duty cycle becomes slightly lower (35%), and this structural difference can be attributed to the weak contact between the stamp and the microfiber. Moreover, due to the curvature of the microfiber, a maximum angular surface coverage of 90° may be reached with this patterning method. Therefore, our results bear witness to the ability of microcontact printing for generating patterned networks of biomolecules even on fragile and non-flat micrometric surfaces.

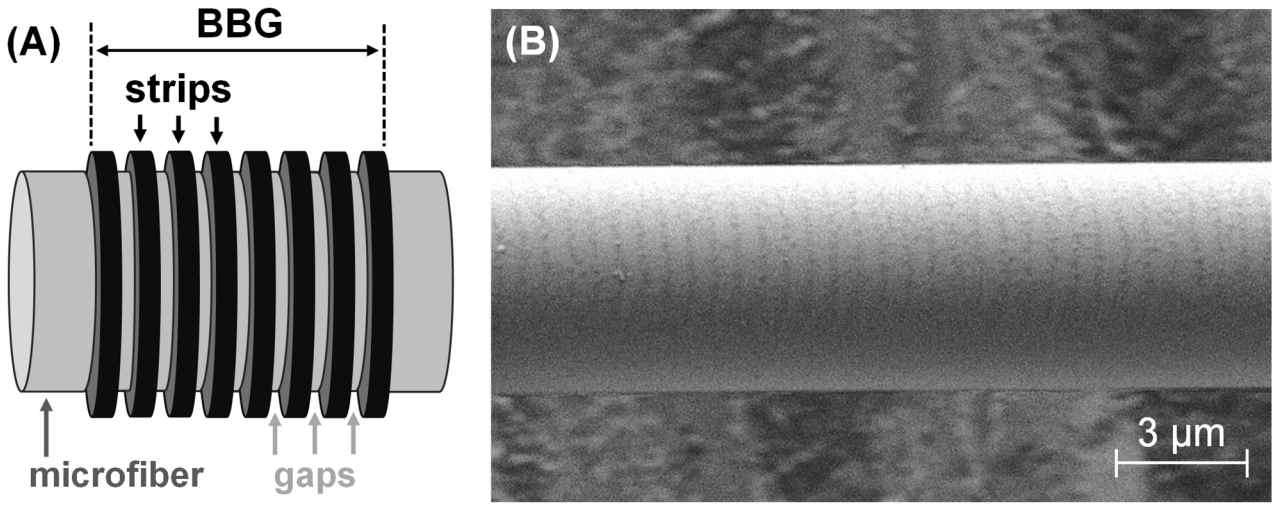

Fig. 3. (A) Scheme of a BBG fabricated on a microfiber and (B) FESEM image of a BSA BBG patterned onto a 5 µm microfiber.

In order to monitor and optimize the fabrication process, we measured the optical response of the BBGs by means of the collection of reflection and transmission spectra at each step of their fabrication and the subsequent biorecognition assay on a 3 µm microfiber. At first, only the reflection peak corresponding to the reference FBG (1564 nm, Fig. 4 i) is observed. An additional intense reflection peak appears at 1537 nm during the BBG stamping step (Fig. S9), which meets the Bragg condition and confirms an effective contact of the grooved stamp on the surface of the microfiber. After the stamping, this peak remains in the reflection spectrum (Fig. 4 ii), which corroborates the transfer of the stamped bioreceptor and the proper structuration of the resulting BBG. This initial BBG peak reaches a -27 dB level respect to the reference, and this reflectivity drop agrees with the lower thickness and refractive index contrast of patterned proteins, compared to the grooved PDMS stamp in the previous stage.

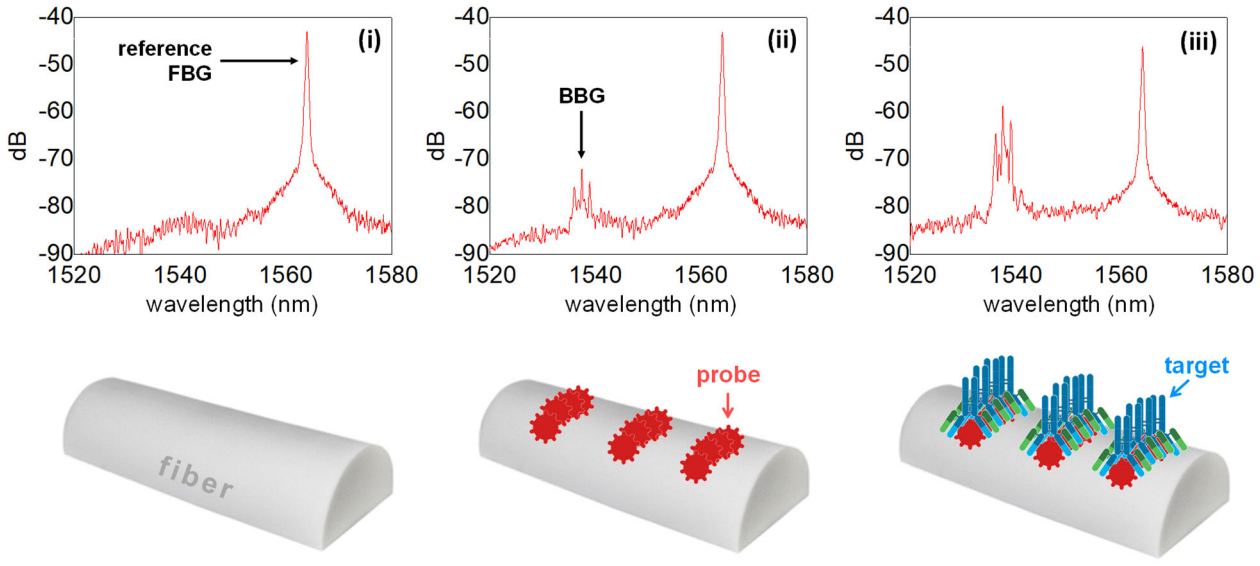

Fig. 4. Experimental reflection spectra obtained at (i) Initial step, (ii) after the patterning a BBG of BSA, and (iii) after incubating specific antiBSA IgGs (10 µg mL^{-1}). Schematic illustrations of the fiber and the BBG at each step is represented below each corresponding spectrum.

Finally, the incubation of selective IgGs on the patterned protein displays an important enhancement of the BBG reflection peak that reaches a -13 dB level respect to the reference (14 dB increase), as shown in Fig. 4 iii. According to the starting hypothesis, this enhancement must come from the greater amount of biological matter in the BBG strips generated by the biorecognition between the patterned probes and their targets in solution. Furthermore, this reflectivity enhancement is not observed after incubating only PBS-T buffer (Fig. S10). It is important to highlight here that this result constitutes the first experimental proof of bioanalytical transduction principle investigated in this study. Besides, the reflectivity of the reference FBG peak was used as a reference signal along the whole process, as well as to monitor any significant optical loss in the system.

3.3 Experimental performance

As a preliminary experimental prove towards real biosensing, we explored how the thickness of the biological layer that constitutes the BBG strips affects the optical response. For that, BBGs of proteins with a range of molecular weights (from 24 to 118 kDa) were patterned on different microfibers, and the intensity of the resulting reflection peak was compared. The results of this experiment (Fig. S11) show that the resulting peak reflectivity increases together with the molecular weight of the proteins (i.e., the amount of matter on the BBG strips), as expected and necessary for the success of this transduction system.

As discussed above, the intensity of the BBG peak in the reflection spectrum is predicted to decay as the diameter of the microfiber increases (Fig. 2B), and only BBG reflectivities produced in microfibers with diameters below 5 microns may be detected with standard equipment. This is a crucial issue since greater analytical signals in the biorecognition transduction will potentially enhance the sensitivity of the resulting bioanalytical systems. As observed in Fig. 5A, the simulated trend is also observed in experimental conditions. The divergencies between both trends were

attributable to the fact that simulations are unable to consider the experimental uncertainty. Although maximum reflectivities for fiber diameters of 2 μm (and below) are displayed by the theoretical calculations, we have experimentally observed that these microfibres are much more fragile and lead to higher optical losses in the BBGs patterning and the subsequent sample incubations. Hence, 3 μm microfiber diameter was considered the best option.

However, although thoroughly checked, negligible changes in the optical response (both in amplitude and wavelength position) were observed for different linear polarizations when experimentally measuring bioreceptor BBGs, even after interacting with high concentrations of their target IgGs. In particular, it was confirmed by experimental results that the Bragg wavelength splitting is only observed in high-contrast gratings, as the ones resulting from the contact between the grooved PDMS and the fiber in the first step of the BBG patterning (Figure S4). It is possible that a random polarization conversion in the grating region is behind the lack of significant polarization effects. Therefore, the polarizing elements were omitted in the optical setup for measuring BBG biorecognition assays in experimental conditions.

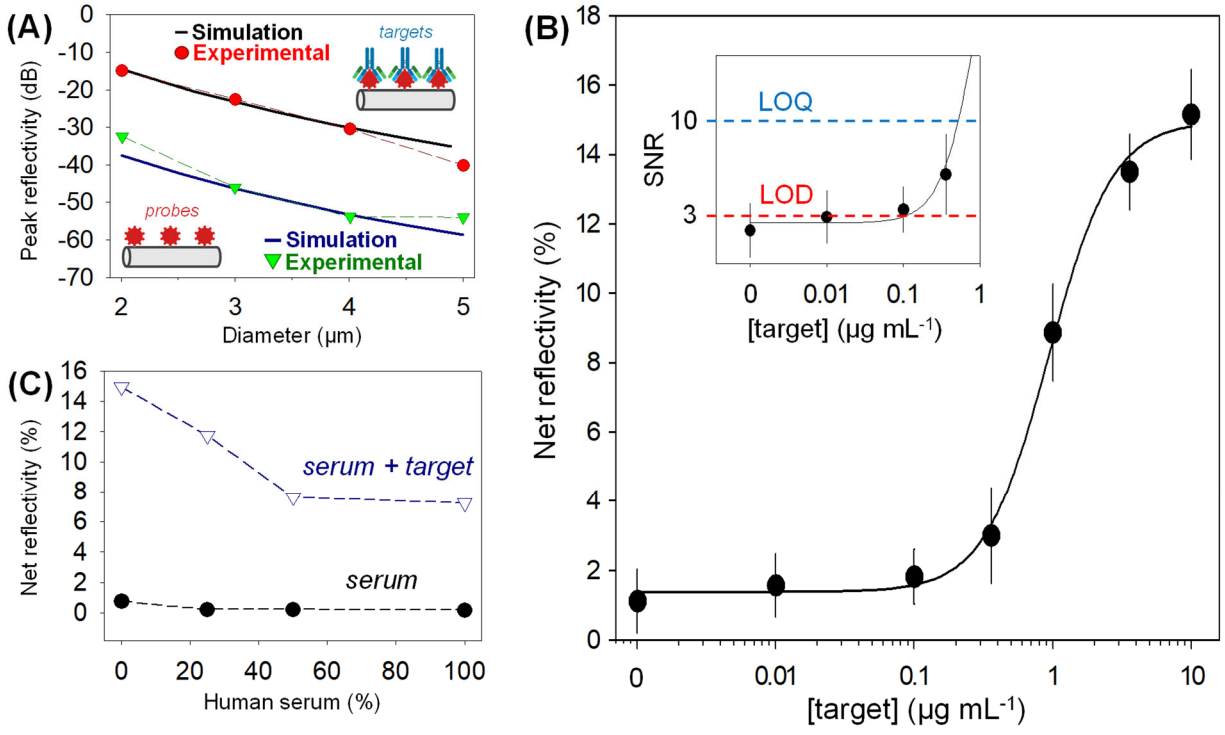

Fig. 5. (A) BBG peak reflectivities of patterned BSA probes before (green triangles) and after (red circles) incubating a solution of specific IgG (10 µg mL^{-1}), for a range of fiber diameters. Blue and black continuous lines represent the corresponding simulated data considering BBG thicknesses of 1 and 10 nm, respectively. **(B)** Experimental dose-response immunoassay curve, fitted to a sigmoidal (logistic 4 parameters) regression. **(C)** Net reflectivity achieved after incubating different dilutions of human serum in PBS-T buffer onto BBGs without (black circles) and with specific IgG (10 µg mL^{-1}, blue empty triangles).

3.4 Immunosensing

The biosensing capabilities were studied by means of an experimental dose-response curve using a representative model immunoassay based on BBGs of patterned BSA probes and specific antiBSA IgGs as targets. A set of 3 µm microfibers were individually fabricated, patterned with the BSA probes, and incubated with different concentrations of target. As shown in Fig. 5B, the increase of the peak reflectivity is proportional to the target concentration, achieves a maximal reflectivity of 15%, and correlates well with the expected trend for a biorecognition dose-response curve (R^2 = 0,997). This indicates that the reproducibility in the fabrication and testing

processes is high. From these results, experimental detection and quantification limits of 0.1 μg mL^{-1} and 0.4 μg mL^{-1}, respectively, of IgG in label-free conditions are inferred. This is a promising sensitivity which is in the range of other recent label-free optical approaches (Chen et al., 2018; Gatterdam et al., 2017; Juste-Dolz et al., 2018; Makhneva et al., 2019).

An important issue in biosensing are the problems associated to non-specific binding (NSB) (Hirst et al., 2008; Mittal et al., 2013). This is especially critical in label-free systems and biological samples, which commonly comprise a high content of biomacromolecules that adsorb on the sensor surface and generate signals that cannot be discriminated from the ones originated by the biorecognition of interest. A unique feature of diffractive bioanalytical systems is their potential to minimize signal contributions generated by NSB (Gatterdam et al., 2017). Unlike specific biorecognition of targets in the probe strips, NSB is a random process prone to take place evenly in the BBG strips and gaps. Therefore, in a first approximation, the reduction in the refractive index contrast generated by the unspecific adsorption on the gaps becomes compensated by the increase in the refractive index contrast caused by the NSB in the strips. To evaluate the effect of NSB, we studied the response of the system with the model immunoassay under a range of dilutions of human serum (7% of non-specific proteins, potentially interfering lipids, etc.) in PBS-T. Fig. 5C shows that reflectivity drops by half when pure human serum containing specific targets is incubated and it increases until it reaches the level of maximum reflectivity (R = 15 %) for pure PBS-T (blue squares). Besides, the same serum dilutions without targets do not involve significant changes in the reflectivity achieved by the BSA pattern itself (Fig. 5C, black squares). These results demonstrate very promising perspectives for label-free detection in complex matrixes, whereas these NSB features could be improved by designing BBGs with a minimal compositional difference between the strips and the gaps.

Another interesting feature of this biosensing system is the easy wavelength tunability of its optical response. The Bragg's wavelength of the BBG reflection peak can be controlled by modifying the fiber diameter, in a first approach. As represented in Fig. 6A, a change in the diameter of the fiber induces a variation of the effective refractive index of the optical mode. Thus, a change in the microfiber diameter results in a Bragg's wavelength shift according to the Bragg condition. Our experimental results using fibers with diameters ranging from 2 to 5 μm match well with the simulations (Fig. 6B), being possible to tune the response within a range of 60 nm (from 1500 to 1560 nm). However, this approach would result in poorer sensitivities for the largest diameters.

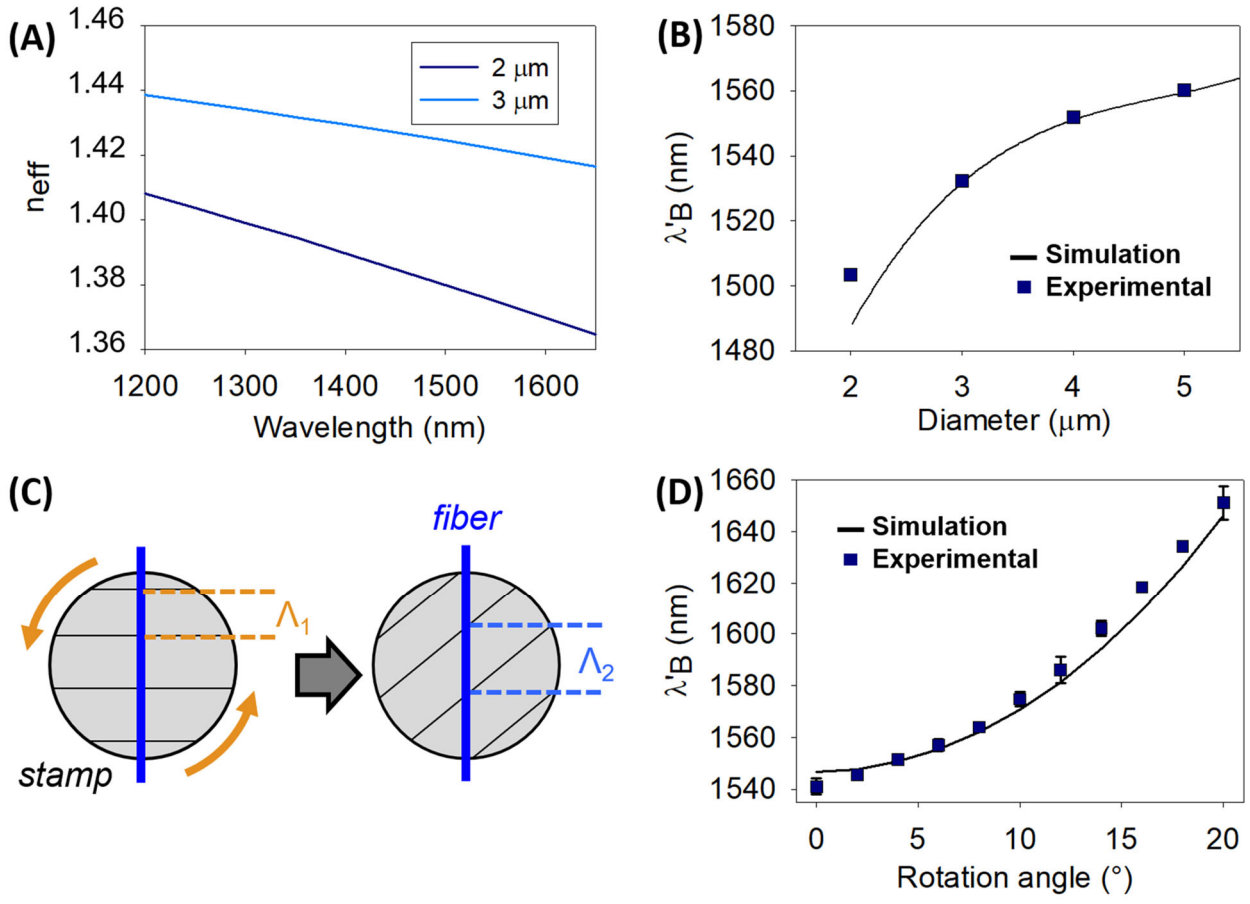

Fig. 6. Tunability of the bioanalytical response. (A) Calculated wavelength dispersion of LP_{01} n_{eff} for two microfiber diameters. (B) Experimental Bragg's wavelength of the BBG peaks (after incubating target IgGs at 10 μg mL^{-1}) in a range of fiber diameters and the corresponding simulated results (strip height of 10 nm). (C) Scheme of the variation of the period by rotating the stamp in the BBG

patterning. (D) Experimental Bragg's wavelength shift measured for different devices. All of them were patterned using a 555 nm period stamp in a 3-micron fiber, by changing the angle between the stamp strips and the axis of the fiber. The simulation shows a sinus trend.

Alternatively, the position of the BBG peak can also be tuned by modifying the BBG period. We found that this parameter can be easily controlled experimentally by just rotating the inked stamp in the stamping step (Fig. 6C), with respect to the longitudinal axis of the microfiber. This approach allows tuning the Bragg's wavelength accurately, since the reflectivity peak shifts towards longer wavelengths when the rotation angle increases. Also, it involves minimal nanofabrication requirements, when compared to creating a specific master substrate for each period. As shown in Fig. 6D, this tunning strategy permits to shift the position of the BBG peak up to 120 nm in 20 degrees.

In addition to provide versatility in terms of the optical instrumentation compatible with this bioanalytical approach, this tunability introduces interesting capabilities for performing multiplexed assays. For example, the reflection peaks of multiple assays could be acquired in a single measurement, and effectively discriminated by combining BBGs with different periods in the same microfiber (Fig. 7A). To explore it, two BBGs were created on a single microfiber with two different stamp rotation angles (5° and 15° degrees), which resulted in different Λ_{BBG} (558 nm and 575 nm, respectively), in experimental immunoassay conditions. As shown in Fig. 7B, two main peaks were obtained, each one of them transducing the biorecognition event of a different assay. The peak at 1615 nm corresponds to the immunoassay with a shorter BBG period (558 nm) and the 1650 nm peak to the longer period one (575 nm). Both peaks can be discriminated and quantified in the reflection spectrum of a single measurement, and this prove aims to open the door for prospective BBG systems integrating multiple BBGs tuned to spread across the reflection spectrum in order to perform and quantify multiple label-free assays for different targets in a single step.

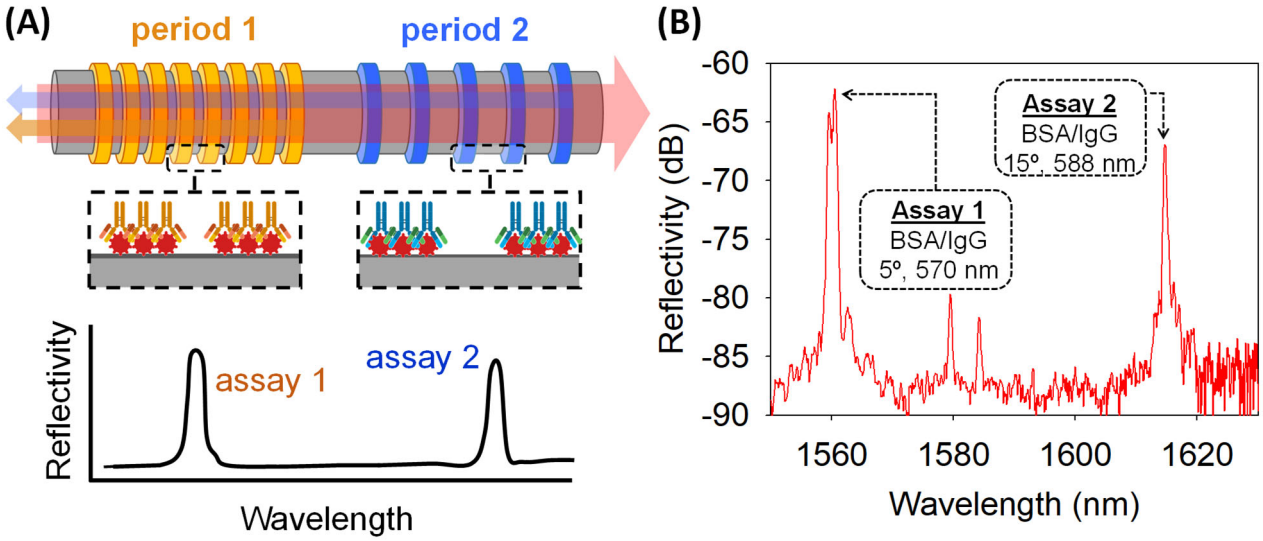

Fig. 7. Assay multiplexing by patterning different BBG periods in a single microfiber. **(A)** Schematic illustration of the approach. **(B)** Experimental reflection spectra obtained with the model immunoassay after incubating the target IgG (10 µg mL^{-1}) in two different BBGs patterned on a single fiber.

5. CONCLUSIONS

This work introduces and demonstrates Bio Bragg Gratings for biosensing, a new physicochemical principle to transduce biorecognition events, based on diffractive networks of bioreceptors patterned on optical waveguides. The results of this theoretical and experimental study support the design, optimization, characterization and fabrication of functional biosensing systems capable of transducing unlabeled immunoassays as a peak in the reflection spectra. The approach is herein implemented in microfibers (1-5 µm in diameter) fabricated from standard optical fibers, which is an extremely inexpensive material that ensures a low optical loss and projects interesting perspectives for integration in telecommunication systems. This work also demonstrates the capability of micro-contact printing to pattern biomacromolecules onto fragile and non-flat microstructures. Different devices were fabricated and tested individually in a model immunoassay based on protein probes and IgG targets, and the results display well-correlated quantitative dose-response

curves in label-free conditions. This biosensing approach presents appealing perspectives to avoid signal contributions from non-specific binding in the analysis of complex biological samples, as shown in this study with human blood serum. Besides, the wavelength response of the sensor can be easily tuned by modifying the microfiber diameter or the period of the biomolecular grating, and the results demonstrate that this tunability provides an interesting solution to perform multiplexed assays on a single fiber. In addition to introduce new biosensing possibilities for fiber-based developments, this investigation provides the basis for a prospective implementation of this transduction system in other waveguide materials and devices to conceive new integrated biosensors.

Acknowledgements

Spanish Ministry of Science and Innovation (CTQ2016-75749-R and TEC2016-80385-P), Agencia Estatal de Investigación and Fondo Europeo de Desarrollo Regional (PID2019-110877GB-I00 and PDI2019-104276RB-I00) and Generalitat Valenciana (PROMETEO/2019/048 and PROMETEO/2017/103). A.J.-D. acknowledges the FPI-UPV 2017 grant program, M.A.-O acknowledges the APSOSTD/2019 program of the GVA.

References

Avella-Oliver, M., Carrascosa, J., Puchades, R., Maquieira, Á., 2017. Diffractive Protein Gratings as Optically Active Transducers for High-Throughput Label-free Immunosensing. Anal. Chem. 89, 9002–9008. https://doi.org/10.1021/acs.analchem.7b01649

Avella-Oliver, M., Ferrando, V., Monsoriu, J.A., Puchades, R., Maquieira, A., 2018. A label-free diffraction-based sensing displacement immunosensor to quantify low molecular weight organic compounds. Anal. Chim. Acta 1033, 173–179. https://doi.org/10.1016/j.aca.2018.05.060

Bekmurzayeva, A., Dukenbayev, K., Shaimerdenova, M., Bekniyazov, I., Ayupova, T.,

Sypabekova, M., Molardi, C., Tosi, D., 2018. Etched fiber bragg grating biosensor functionalized with aptamers for detection of thrombin. Sensors (Switzerland) 18. https://doi.org/10.3390/s18124298

Bhattacharyya, I.M., Cohen, S., Shalabny, A., Bashouti, M., Akavayov, B., Shalev, G., 2019. Specific and label-free immunosensing of protein-protein interactions with silicon-based immunoFETs. Biosens. Bioelectron. 132, 143–161. https://doi.org/10.1016/j.bios.2019.03.003

Birks, T.A., Li, Y.W., 1992. The Shape of Fiber Tapers. J. Light. Technol. 10, 432–438. https://doi.org/10.1109/50.134196

Cao, Y., Wang, W., Guo, T., Ran, Y., Feng, X., Guan, B.-O., Yao, J., 2017. High-resolution and temperature-compensational HER2 antigendetection based on microwave photonic interrogation. Sens. Act. B. 245, 583-589. http://dx.doi.org/10.1016/j.snb.2017.01.085

Chen, W.T., Li, S.S., Chu, J.P., Feng, K.C., Chen, J.K., 2018. Fabrication of ordered metallic glass nanotube arrays for label-free biosensing with diffractive reflectance. Biosens. Bioelectron. 102, 129–135. https://doi.org/10.1016/j.bios.2017.10.023

Chen, Y., Liu, J., Yang, Z., Wilkinson, J.S., Zhou, X., 2019. Optical biosensors based on refractometric sensing schemes: A review. Biosens. Bioelectron. 144, 111693. https://doi.org/10.1016/j.bios.2019.111693

Delgado-Pinar, M., Shi, Q., Poveda-Wong, L., Delgado-Pinar, E., Xu, B., Zhao, J., Cruz, J.L., Andrés, M. V., 2017. Oligonucleotide-Hybridization Fiber-Optic Biosensor Using a Narrow Bandwidth Long Period Grating. IEEE Sens. J. 17, 5503–5509. https://doi.org/10.1109/JSEN.2017.2723759

Erdogan, T., 1997, Fiber grating spectra. J. Light. Technol, 15, 1277-1294. https://doi.org/10.1109/50.618322

Escorihuela, J., González-Martínez, M.Á., López-Paz, J.L., Puchades, R., Maquieira, Á., Gimenez-Romero, D., 2015. Dual-polarization interferometry: A novel technique

to light up the nanomolecular world. Chem. Rev. https://doi.org/10.1021/cr5002063

Freeman, N.J., Peel, L.L., Swann, M.J., Cross, G.H., Reeves, A., Brand, S., Lu, J.R., 2004. Real time, high resolution studies of protein adsorption and structure at the solid-liquid interface using dual polarization interferometry. J. Phys. Condens. Matter 16, 0–4. https://doi.org/10.1088/0953-8984/16/26/023

Frutiger, A., Blickenstorfer, Y., Bischof, S., Forró, C., Lauer, M., Gatterdam, V., Fattinger, C., Vörös, J., 2019. Principles for Sensitive and Robust Biomolecular Interaction Analysis: The Limits of Detection and Resolution of Diffraction-Limited Focal Mology raphy. Phys. Rev. Appl. 11, 1. https://doi.org/10.1103/PhysRevApplied.11.014056

Frutiger, A., Tschannen, C.D., Blickenstorfer, Y., Reichmuth, A.M., Fatttinger, C., Vörös, J., 2020. Image reversal reactive immersion lithography improves the detection limit of focal mology raphy: erratum. Opt. Lett. 45, 918. https://doi.org/10.1364/ol.45.000918

Gatterdam, V., Frutiger, A., Stengele, K.P., Heindl, D., Lübbers, T., Vörös, J., Fattinger, C., 2017. Focal mology raphy is a new method for the in situ analysis of molecular interactions in biological samples. Nat. Nanotechnol. 12, 1089–1095. https://doi.org/10.1038/nnano.2017.168

Goh, J.B., Loo, R.W., Goh, M.C., 2005. Label-free monitoring of multiple biomolecular binding interactions in real-time with diffraction-based sensing. Sensors Actuators, B Chem. 106, 243–248. https://doi.org/10.1016/j.snb.2004.08.003

Goh, J.B., Loo, R.W., McAloney, R.A., Goh, M.C., 2002. Diffraction-based assay for detecting multiple analytes. Anal. Bioanal. Chem. 374, 54–56. https://doi.org/10.1007/s00216-002-1478-5

Hirst, E.R., Yuan, Y.J., Xu, W.L., Bronlund, J.E., 2008. Bond-rupture immunosensors-A review. Biosens. Bioelectron. 23, 1759–1768.

https://doi.org/10.1016/j.bios.2008.02.002
Juste-Dolz, A., Avella-Oliver, M., Puchades, R., Maquieira, A., 2018. Indirect microcontact printing to create functional patterns of physisorbed antibodies. Sensors (Switzerland) 18. https://doi.org/10.3390/s18093163
Lamping, S., Buten, C., Ravoo, B.J., 2019. Functionalization and Patterning of Self-Assembled Monolayers and Polymer Brushes Using Microcontact Chemistry. https://doi.org/10.1021/acs.accounts.9b00041
Langer, J., de Aberasturi, D.J., Aizpurua, J., Alvarez-Puebla, R.A., Auguié, B., Baumberg, J.J., Bazan, G.C., Bell, S.E.J., Boisen, A., Brolo, A.G., Choo, J., Cialla-May, D., Deckert, V., Fabris, L., Faulds, K., Javier García de Abajo, F., Goodacre, R., Graham, D., Haes, A.J., Haynes, C.L., Huck, C., Itoh, T., Käll, M., Kneipp, J., Kotov, N.A., Kuang, H., Le Ru, E.C., Lee, H.K., Li, J.F., Ling, X.Y., Maier, S.A., Mayerhöfer, T., Moskovits, M., Murakoshi, K., Nam, J.M., Nie, S., Ozaki, Y., Pastoriza-Santos, I., Perez-Juste, J., Popp, J., Pucci, A., Reich, S., Ren, B., Schatz, G.C., Shegai, T., Schlücker, S., Tay, L.L., George Thomas, K., Tian, Z.Q., van Duyne, R.P., Vo-Dinh, T., Wang, Y., Willets, K.A., Xu, C., Xu, H., Xu, Y., Yamamoto, Y.S., Zhao, B., Liz-Marzán, L.M., 2020. Present and future of surface-enhanced Raman scattering. ACS Nano 14, 28–117. https://doi.org/10.1021/acsnano.9b04224
Liu, J., Jalali, M., Mahshid, S., Wachsmann-Hogiu, S., 2020. Are plasmonic optical biosensors ready for use in point-of-need applications? Analyst. https://doi.org/10.1039/c9an02149c
Liu, T., Liang, L.-L., Xiao, P., Sun, L.-P., Huang, Y.-Y., Ran, Y., Jin, L., Guan, B.-O., 2018. A label-free cardiac biomarker immunosensor based on phase-shiftedmicrofiber Bragg grating. Biosens. Bioelectron. 100, 155-160. https://doi.org/10.1016/j.bios.2017.08.061
Loyez, M., Hassan, E.M., Lobry, M., Liu, F., Caucheteur, C., Wattiez, R., Derosa, M.C., Willmore, W.G., Albert, J., 2020. Rapid Detection of Circulating Breast Cancer

559 Cells Using a Multiresonant Optical Fiber Aptasensor with Plasmonic
560 Amplification. ACS Sensors 5, 454–463.
561 https://doi.org/10.1021/acssensors.9b02155
562 Mahmoudpour, M., Ezzati Nazhad Dolatabadi, J., Torbati, M., Pirpour Tazehkand, A.,
563 Homayouni-Rad, A., de la Guardia, M., 2019. Nanomaterials and new
564 biorecognition molecules based surface plasmon resonance biosensors for
565 mycotoxin detection. Biosens. Bioelectron. 143, 111603.
566 https://doi.org/10.1016/j.bios.2019.111603
567 Makhneva, E., Farka, Z., Pastucha, M., Obrusník, A., Horáčková, V., Skládal, P.,
568 Zajíčková, L., 2019. Maleic anhydride and acetylene plasma copolymer surfaces
569 for SPR immunosensing. Anal. Bioanal. Chem. 411, 7689–7697.
570 https://doi.org/10.1007/s00216-019-01979-9
571 Malachovská, V., Ribaut, C., Voisin, V., Surin, M., Leclère, P., Wattiez, R., Caucheteur,
572 C., 2015. Fiber-Optic SPR Immunosensors Tailored to Target Epithelial Cells
573 through Membrane Receptors. Anal. Chem. 87, 5957–5965.
574 https://doi.org/10.1021/acs.analchem.5b00159
575 Mittal, S., Wong, I.Y., Yanik, A.A., Deen, W.M., Toner, M., 2013. Discontinuous
576 nanoporous membranes reduce non-specific fouling for immunoaffinity cell
577 capture. Small 9, 4207–4214. https://doi.org/10.1002/smll.201300977
578 Nootchanat, S., Jaikeandee, W., Yaiwong, P., Lertvachirapaiboon, C., Shinbo, K.,
579 Kato, K., Ekgasit, S., Baba, A., 2019. Fabrication of Miniature Surface Plasmon
580 Resonance Sensor Chips by Using Confined Sessile Drop Technique. ACS Appl.
581 Mater. Interfaces 11, 11954–11960. https://doi.org/10.1021/acsami.9b01617
582 Prasad, A., Choi, J., Jia, Z., Park, S., Gartia, M.R., 2019. Nanohole array plasmonic
583 biosensors: Emerging point-of-care applications. Biosens. Bioelectron. 130, 185–
584 203. https://doi.org/10.1016/j.bios.2019.01.037
585 Rumpf, R.C., Garcia, C.R., Berry, E.A., Barton, J.H., 2014. Finite-Difference Frequency-
586 Domain Algorithm for Modeling Electromagnetic Scattering from General

587 Anisotropic Objects. Prog. Electromagn. Res., Vol. 61, 55-67.
588 https://doi.org/10.2528/PIERB14071606
589 Sancho-Fornes, G., Avella-Oliver, M., Carrascosa, J., Fernandez, E., Brun, E.M.,
590 Maquieira, Á., 2019. Disk-based one-dimensional photonic crystal slabs for
591 label-free immunosensing. Biosens. Bioelectron. 126, 315–323.
592 https://doi.org/10.1016/j.bios.2018.11.005
593 Schneider, A.K., Niemeyer, C.M., 2018. DNA Surface Technology: From Gene Sensors
594 to Integrated Systems for Life and Materials Sciences. Angew. Chemie - Int. Ed.
595 57, 16959–16967. https://doi.org/10.1002/anie.201811713
596 Sridevi, S., Vasu, K.S., Asokan, S., Sood, A.K., 2015. Sensitive detection of C-reactive
597 protein using opticalfiber Bragggratings. Biosens. Bioelectron. 65, 251-256.
598 https://doi.org/10.1016/j.bios.2014.10.033
599 Sypabekova, M., Korganbayev, S., González-Vila, Á., Caucheteur, C., Shaimerdenova,
600 M., Ayupova, T., Bekmurzayeva, A., Vangelista, L., Tosi, D., 2019. Functionalized
601 etched tilted fiber Bragg grating aptasensor for label-free protein detection.
602 Biosens. Bioelectron. 146, 1–9. https://doi.org/10.1016/j.bios.2019.111765
603 Wang, J., Sanchez, M.M., Yin, Y., Herzer, R., Ma, L., Schmidt, O.G., 2020. Silicon-
604 Based Integrated Label-Free Optofluidic Biosensors: Latest Advances and
605 Roadmap. Adv. Mater. Technol. 5. https://doi.org/10.1002/admt.201901138
606 Wang, X., Sperling, M., Reifarth, M., Böker, A., 2020. Shaping Metallic Nanolattices:
607 Design by Microcontact Printing from Wrinkled Stamps. Small 16, 1–8.
608 https://doi.org/10.1002/smll.201906721
609 Wang, X.D., Wolfbeis, O.S., 2020. Fiber-Optic Chemical Sensors and Biosensors
610 (2015-2019). Anal. Chem. 92, 397–430.
611 https://doi.org/10.1021/acs.analchem.9b04708
612 Wong, X.Y., Sena-Torralba, A., Álvarez-Diduk, R., Muthoosamy, K., Merkoçi, A., 2020.
613 Nanomaterials for Nanotheranostics: Tuning Their Properties According to
614 Disease Needs. ACS Nano 14, 2585–2627.

https://doi.org/10.1021/acsnano.9b08133

Xu, L., Shoaie, N., Jahanpeyma, F., Zhao, J., Azimzadeh, M., Al–Jamal, K.T., 2020. Optical, electrochemical and electrical (nano)biosensors for detection of exosomes: A comprehensive overview. Biosens. Bioelectron. 161. https://doi.org/10.1016/j.bios.2020.112222

Yariv, A., Yeh, P, 2007. Photonics: optical electronics in modern communications. Volume 6. New York: Oxford university press.

Zhang, L., Ying, Y., Li, Y., Fu, Y., 2020. Integration and synergy in protein-nanomaterial hybrids for biosensing: Strategies and in-field detection applications. Biosens. Bioelectron. 154, 112036. https://doi.org/10.1016/j.bios.2020.112036

Zhao, Y., Hu, X. guang, Hu, S., Peng, Y., 2020. Applications of fiber-optic biochemical sensor in microfluidic chips: A review. Biosens. Bioelectron. 166, 112447. https://doi.org/10.1016/j.bios.2020.112447

Zhao, Y., Tong, R. jie, Xia, F., Peng, Y., 2019. Current status of optical fiber biosensor based on surface plasmon resonance. Biosens. Bioelectron. 142, 111505. https://doi.org/10.1016/j.bios.2019.111505

Zhu, Z., Brown, T. G., 2002. Full-vectorial finite-difference analysis of microstructured optical fibers. Opt. Express 10, 853–864. https://doi.org/10.1364/OE.10.000853

Supplementary information for:

BIO BRAGG GRATINGS ON MICROFIBERS FOR LABEL-FREE BIOSENSING

Augusto Juste-Dolz[1], Martina Delgado-Pinar[2], Miquel Avella-Oliver*[,1,4], Estrella Fernández[1], Daniel Pastor[3], Miguel V. Andrés[2], Ángel Maquieira*[,1,4]

[1] Instituto Interuniversitario de Investigación de Reconocimiento Molecular y Desarrollo Tecnológico (IDM), Universitat Politècnica de València, Universitat de València, 46022 Valencia, Spain.
[2] Department of Applied Physics and Electromagnetism-ICMUV, Universitat de València, Burjassot 46100, Spain.
[3] Photonics Research Labs, Universitat Politècnica de València, 46021 Valencia, Spain.
[4] Departamento de Química, Universitat Politècnica de València, 46022 Valencia, Spain.

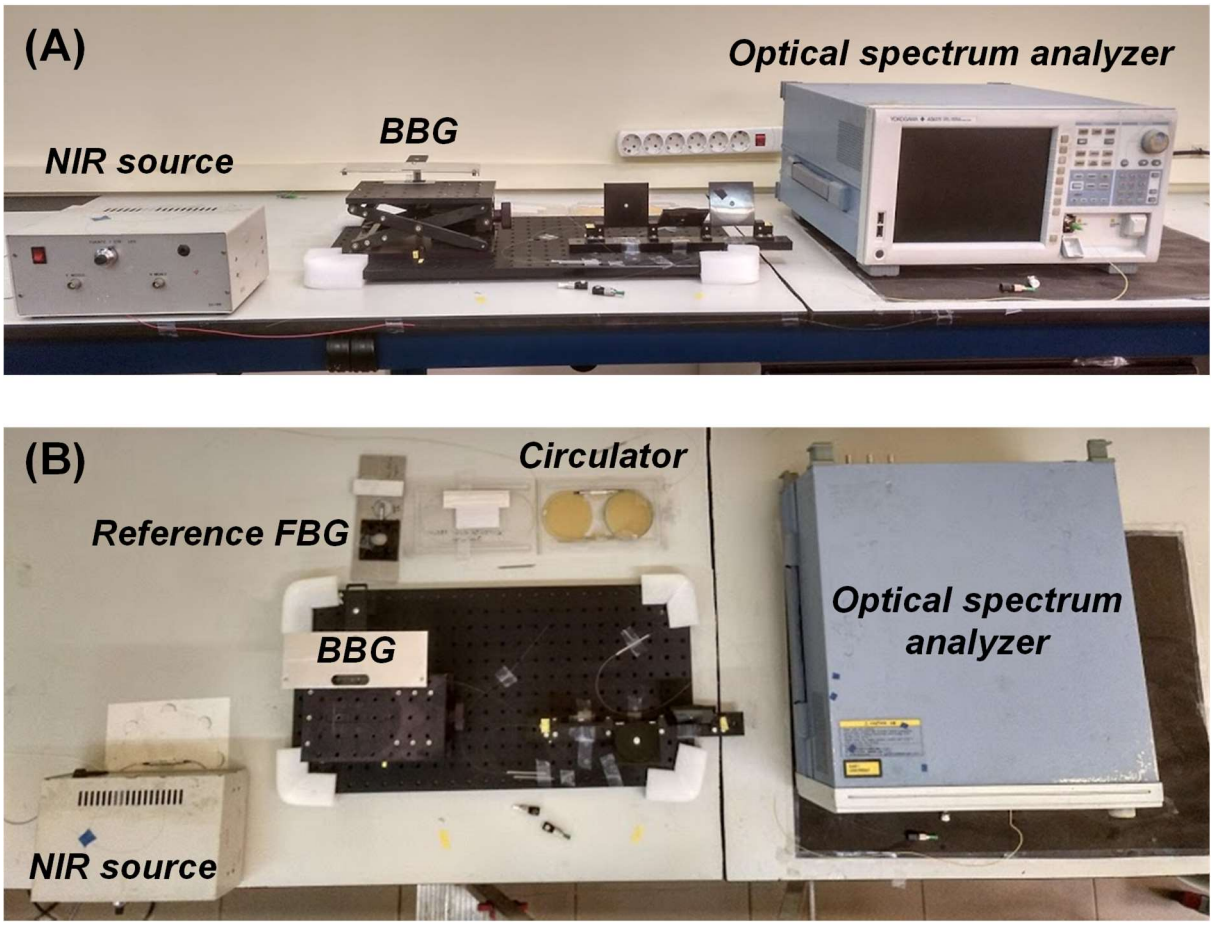

Figure S1. Front (A) and top (B) view of the optical setup used for the measurement and characterization of the BBGs.

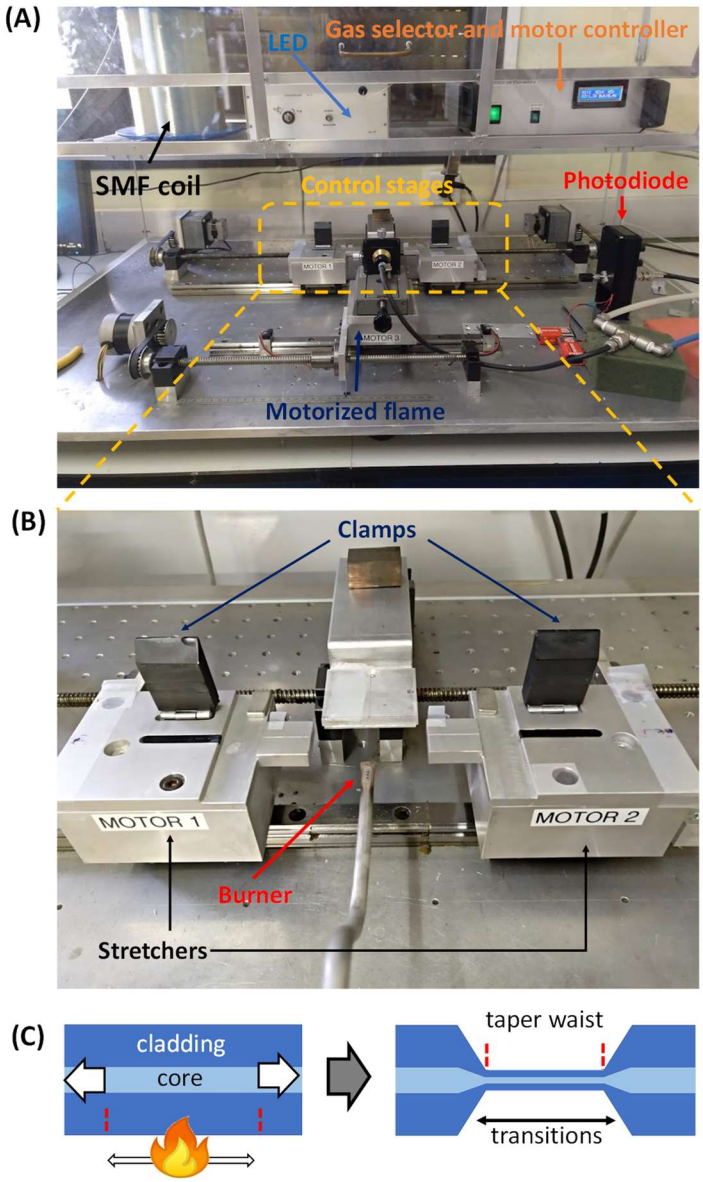

Figure S2. (A) Custom tapering rig station used for the fabrication of tapered optical fibers. The system is fully automatized and it is composed by two gas flow controllers (oxygen and butane) and three motor controllers, one manages the speed of the sweeping flame and the two others control motor the pulling speed of the fiber. An IR LED and an InGaAs photodiode were used for monitoring the losses during taper fabrication. **(B)** Zoomed picture of the stretchers (where the fiber is clamped) and the burner. **(C)** Scheme of the taper fabrication. A single-mode fiber is peeled off, cleaned with acetone, and clamped onto the motorized stretchers. Next, the fiber is stretched while the flame sweeps along the fiber. As a result, the fiber reaches the plastic deformation temperature of the silica, and the stretching narrows the diameter of the fiber, while maintaining the scale of its internal structure and shape. After fabrication, three regions can be identified: the taper waist (with a uniform, reduced diameter along several centimeters), the non-modified region with the original diameter, and the taper transitions (which are the transition regions from original to final diameters, typically several centimeters long). The shape and length of these transitions can be designed on demand, within certain limits.

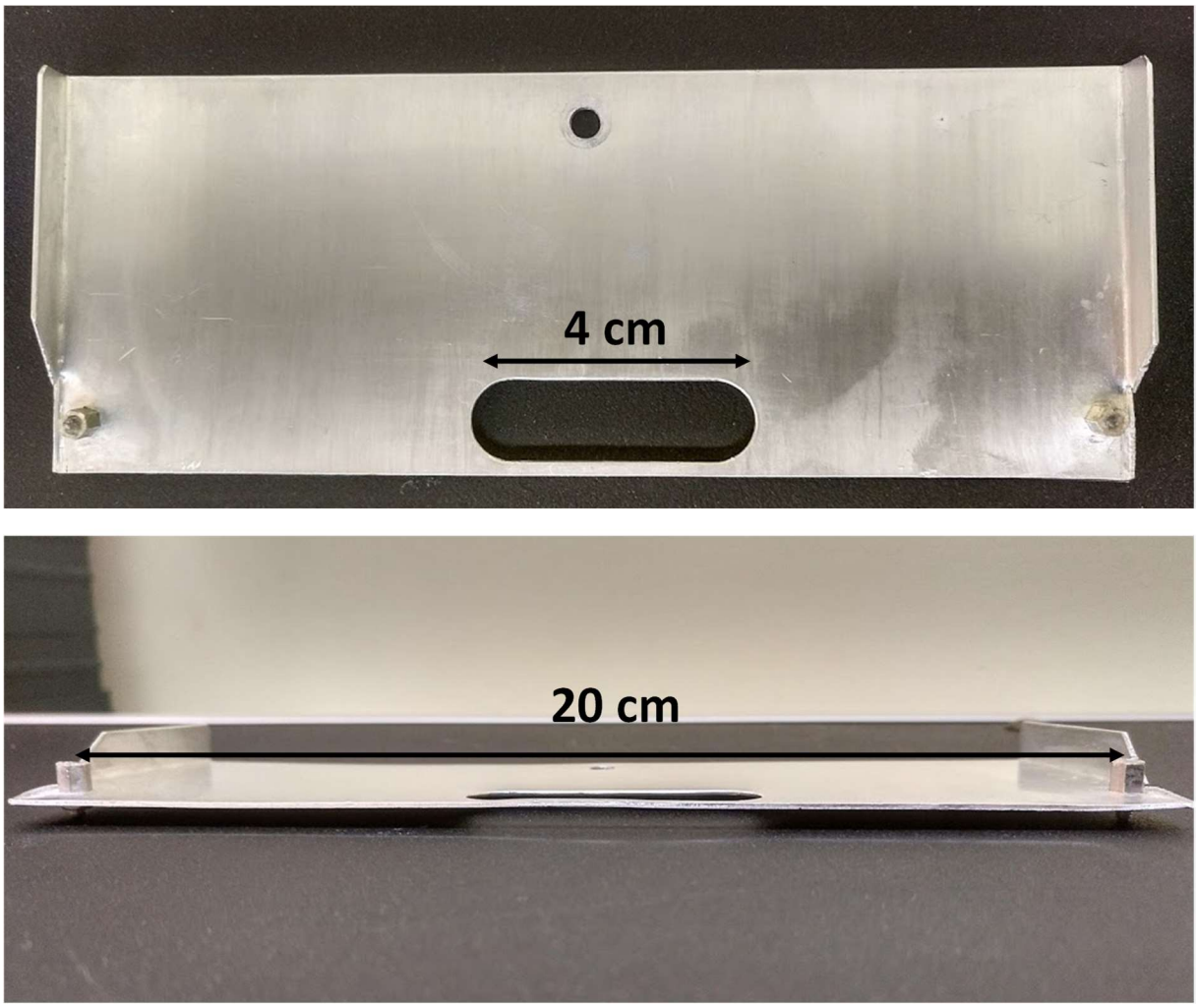

Figure S3. Pictures taken from two different perspectives (top and side) of the custom holder fabricated to keep and manipulate the microfiber. The holder is made of aluminum and has two small cylindrical platforms placed at both ends for fixing the fiber. A 4-centimeter length hole was generated in the middle distance between both platforms to facilitate the contact between the stamp and the hanged fiber. For our experiments, the total length of the tapers including the taper transitions was 20 cm (length of the waist: 2 cm).

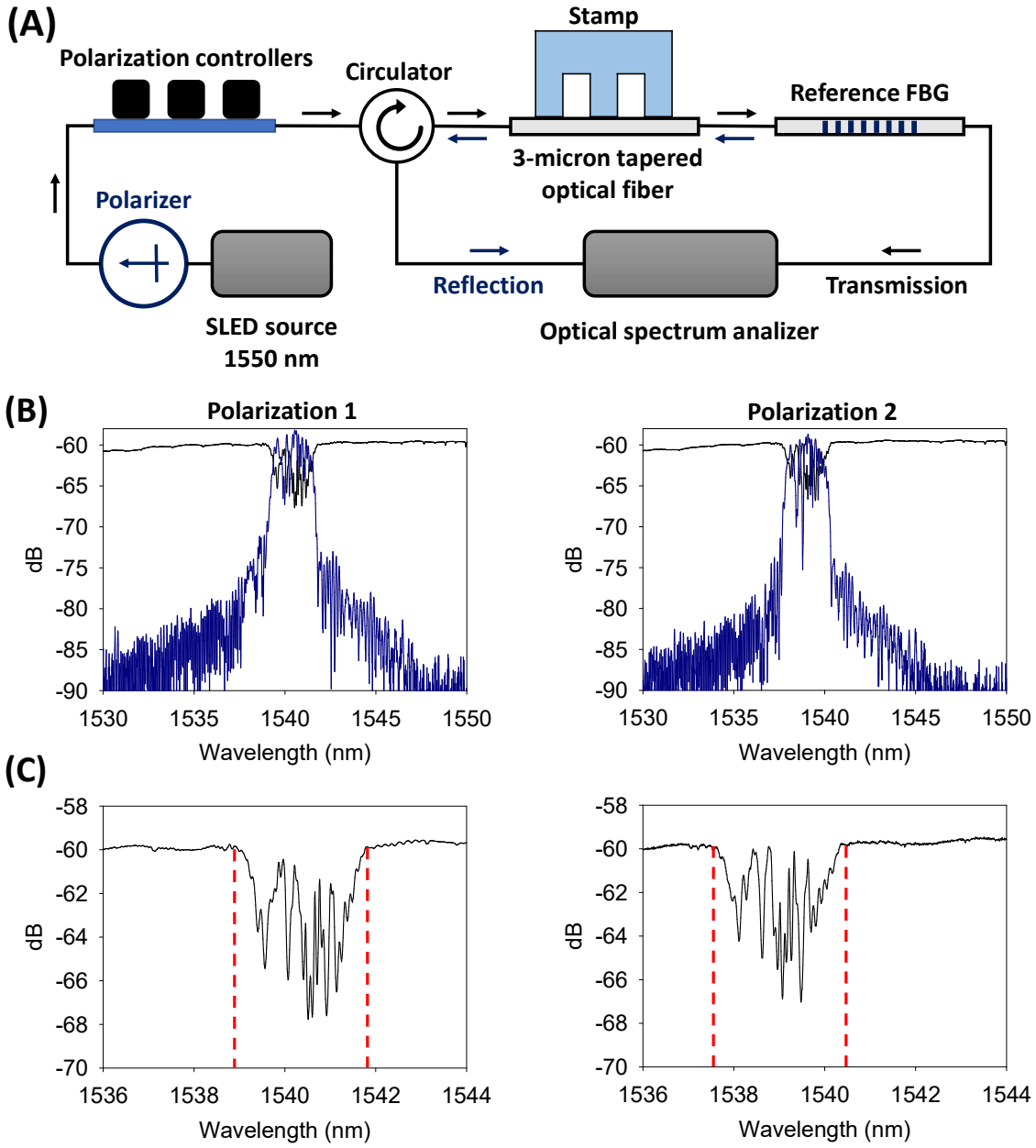

Figure S4. Experimental results on the polarization dependence. **(A)** Scheme of the optical setup used for studying the polarization effect in the system. An in-fiber linear polarizer (Thorlabs, operation wavelength 1550 nm, bandwidth 50 nm) and polarization controllers (Thorlabs, operation wavelength 1550 nm, 56 mm loop) were included after the output of the source to control its linear polarization. **(B)** Reflection (bottom blue line) and transmission (top black line) spectra experimentally obtained at two different linear polarizations for a 3 µm fiber in contact with a grooved PDMS stamp. **(B)** Zoomed view of the transmission notches in the corresponding figures above.

Note that Bragg wavelength of the peak corresponding to the grooved PDMS stamp clearly changes together with the polarization (longer for polarization 1, and shorter for 2). This fact indicates a birefringence caused by the different refractive index of the polarization modes of the microfiber and the asymmetry introduced by the lateral contact of the PDMS stamp on the microfiber.

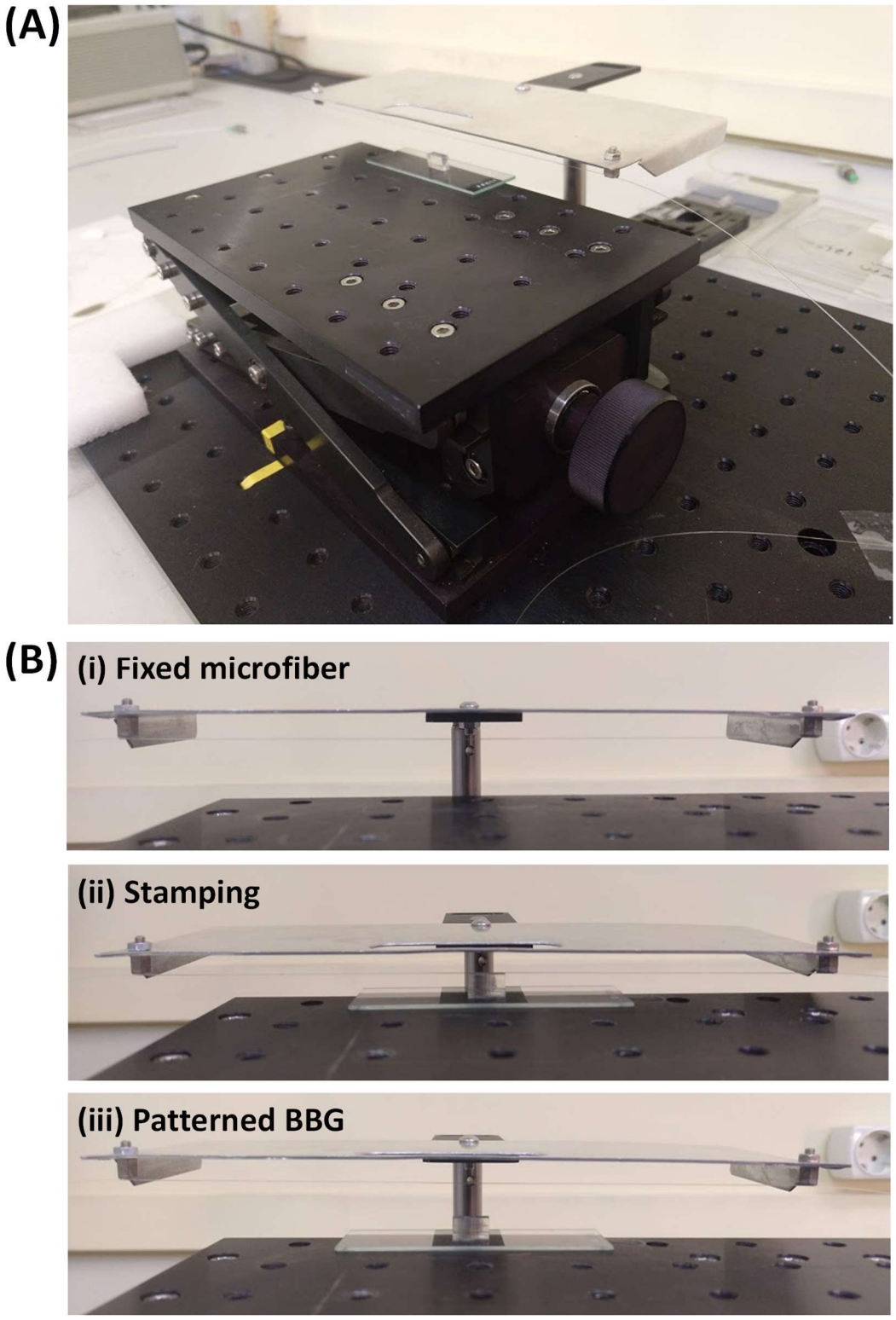

Figure S5. (A) Mechanical elevator used to uplift the inked stamps in the stamping stage of the BBGs fabrication by microcontact printing. **(B)** Real images of the stamping system at the different steps of the BBG fabrication. At initial step **(i)**, the microfiber is fixed in the holder and held just above the elevator. Next, the stamp is placed and oriented right below the microfiber, and the stamp is uplifted until its grooved side becomes in contact with the microfiber **(ii).** Finally, the stamp and the microfiber are separated and a BBG becomes patterned **(iii)**.

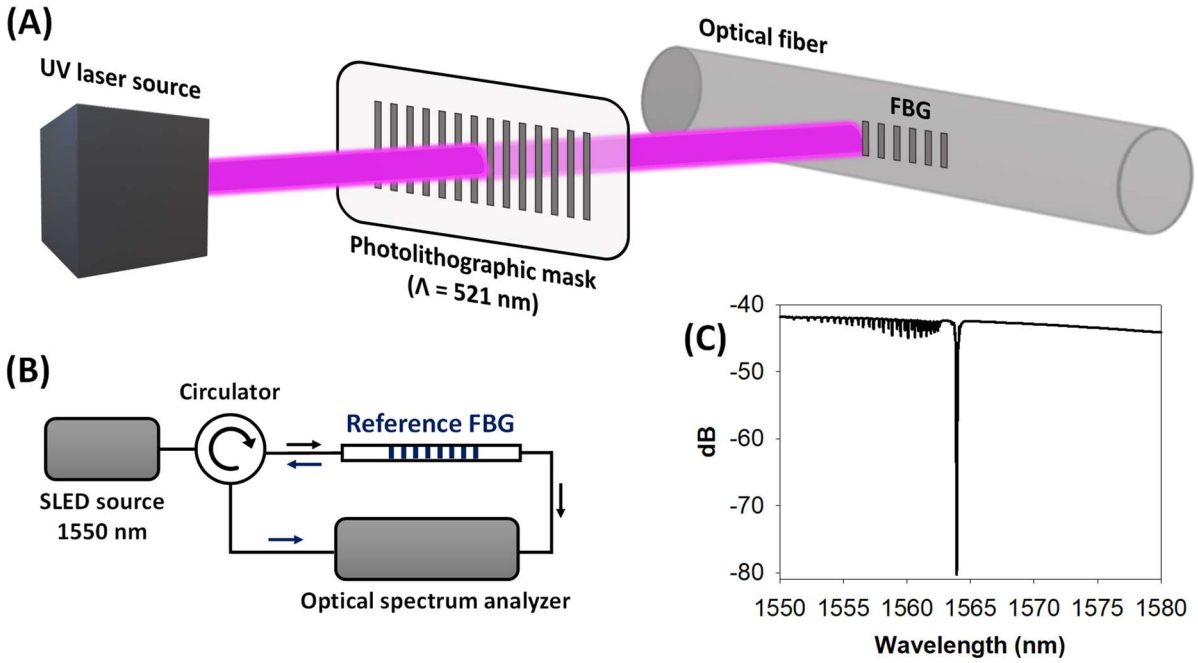

Figure S6. (A) Schematic illustration of the fabrication process of a Fiber Bragg Grating (FBG) used for the reference signals. A CW frequency double Ar laser (λ = 244 nm) irradiates a photolithographic phase mask generating an interferometric UV pattern with the desired pitch for the FBG. A section of a bare boron codoped photosensitive fiber (Fibercore PS1550) is located within the focal length of the interferometric UV pattern, which generates a permanent modulation in the refractive index of the fiber core material. The laser beam sweeps along the length of the fiber, thus the length of the FBG can be of several cm long (in our case, 10 mm). Our FBG was located at 1564.09 nm, with bandwidth < 1 nm and a minimum transmittance of -36 dB, see Figure S6c. (**B)** All-fiber optical circuit used to characterize the FBG. A custom superLED source centered at 1550 nm (1,3 mW, bandwidth > 100 nm) provided the light launched to the FBG. A circulator (Thorlabs, central wavelength: 1550 nm, bandwidth: 90 nm) was placed before the FBG to allow the measurement of the reflection spectrum**. (C)** Transmission spectrum of the reference FBG measured with an AQ6370D optical spectrum analyser from Yokogawa (Tokyo, Japan). As it is shown, the Bragg's wavelength of the FBG is observed at 1564 nm, the notches located at the blue side of the transmission spectrum correspond to the light coupled to different cladding modes of the fiber.

Supplementary Information 7:

The equivalence between logarithmic and linear scale of the transmission and reflection spectrum levels was calculated as follows:

$$dB = 10 \cdot \log_{10}\left(\frac{P_1}{P_0}\right)$$

where dB stands for the logarithmic scale, P_1 stands for the intensity level in linear scale, and P_0 is the instrumentation reference power level.

The logarithmic and linear reflection spectra are shown in Figure S11. The area of the reflection peaks associated to the bioreceptor BBGs and the reference FBG were obtained by numerical integration of the linear traces, and this area corresponds to the total optical power reflected by each grating. The reflectivity of the BBG was referenced to that of the FBG to separate the reflectivity increase due to the biorecognition event, from any broadband optical loss induced along the fabrication and immunosensing with the BBGs. To do so, we employed the following equation:

$$R = \frac{A_{BG}}{A_{REF}} \cdot 100$$

where A_{BG} and A_{REF} are the areas of the reflection peaks attributed to the BBG and the reference FBG, respectively.

Finally, the change of reflectivity due to the biorecognition assay (net reflectivities) were estimated by subtracting the reflectivity of the BBG generated by the probes (R_{probes}), to the reflectivity achieved by the BBG after target incubation ($R_{targets}$):

$$R_{net} = R_{targets} - R_{probes}$$

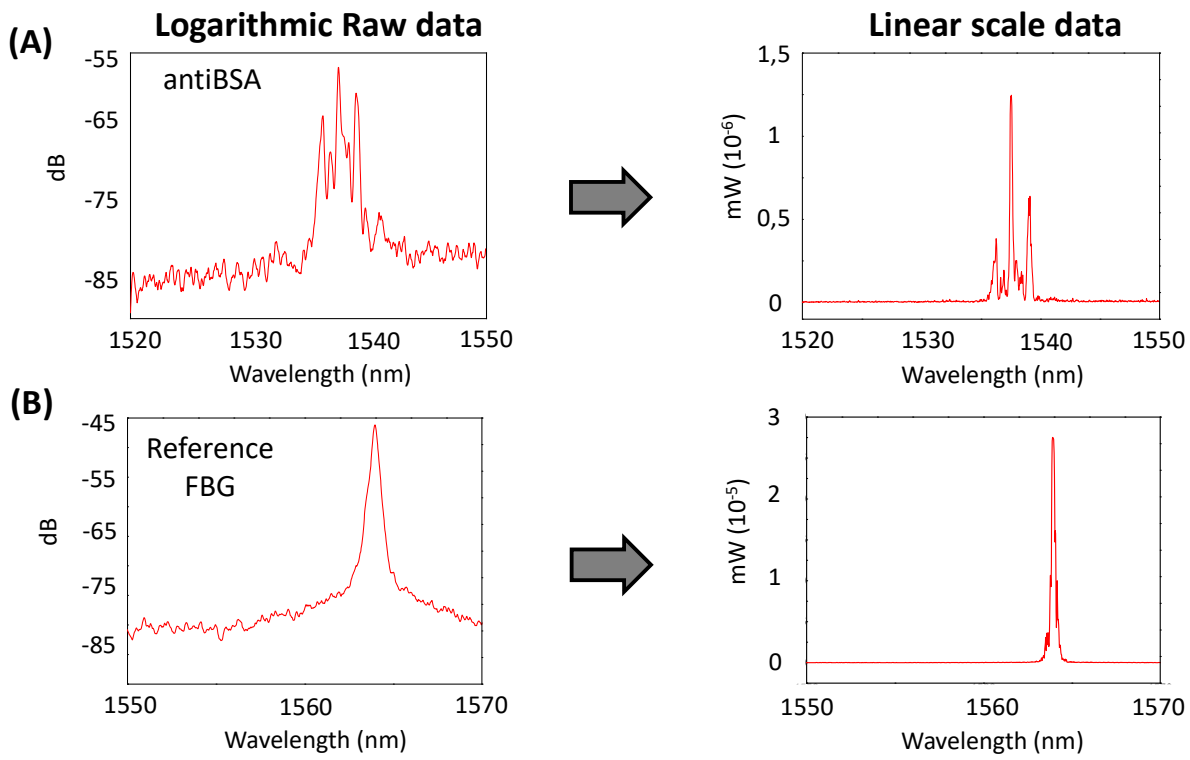

Figure S8. (A) Reflection spectrum with logarithmic scale (left) measured after the target IgG incubation (10 µg·mL^{-1}) and the corresponding spectrum transformed into linear scale (right). **(B)** Reflection spectrum of the reference FBG (left) and the corresponding spectrum in linear scale (right).

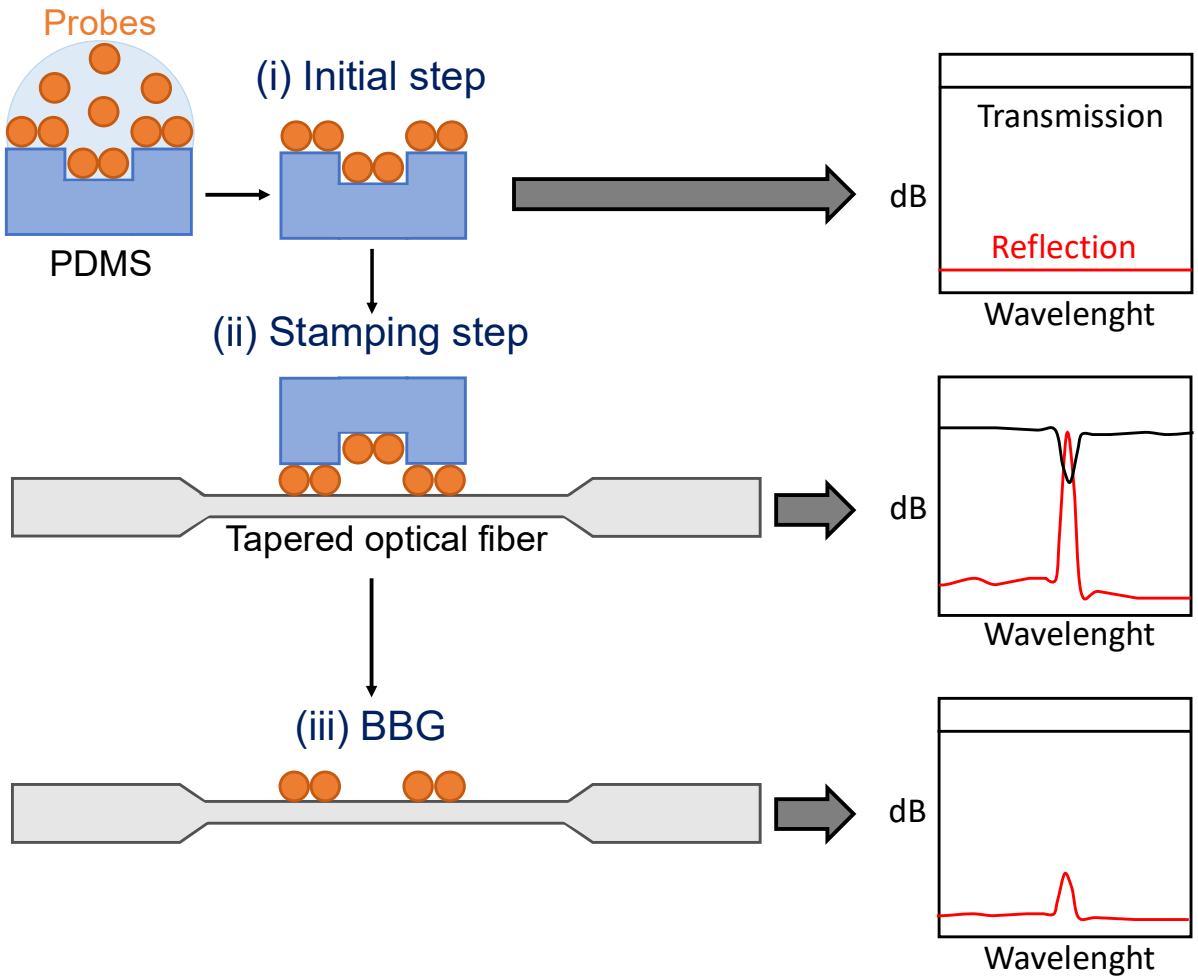

Figure S9. Schematic illustration of the bioreceptor BBGs patterning process on the microfibers by microcontact printing. The transmission and reflection spectra were acquired as a feedback system to monitor and check the success of the patterning process at each step. At the initial stage **(i)** grooved PDMS stamps are inked with the probe solution, and before their stamping on the microfiber, the transmission and reflection spectra are flat and their levels are defined by the taper losses (< 1dB). Next, the inked PDMS structure is stamped on the microfiber **(ii)**. The contact between the microfiber and the stamp introduces some temporary loss (thus, the transmission level decreases), and more importantly it leads to an intense reflection peak whose wavelength (1537 nm) meets the Bragg condition:

$$\lambda'_B = 2n_{eff} \cdot \Lambda_{BBG}$$

where λ'_B is the Bragg's wavelength, n_{eff} is the refractive index of the fundamental mode at λ'_B, and Λ_{BBG} is the period of the grating (555 nm). This intense reflection peak appears together with its corresponding notch in the transmission spectrum at the same wavelength. Finally, after separating the stamp from the microfiber **(iii)**, a weaker reflection peak (and a negligible transmission notch) at the same wavelength remains on the spectra, which confirms the transfer of the bioreceptor probes from the stamp to the microfiber surface and their proper periodic structuration.

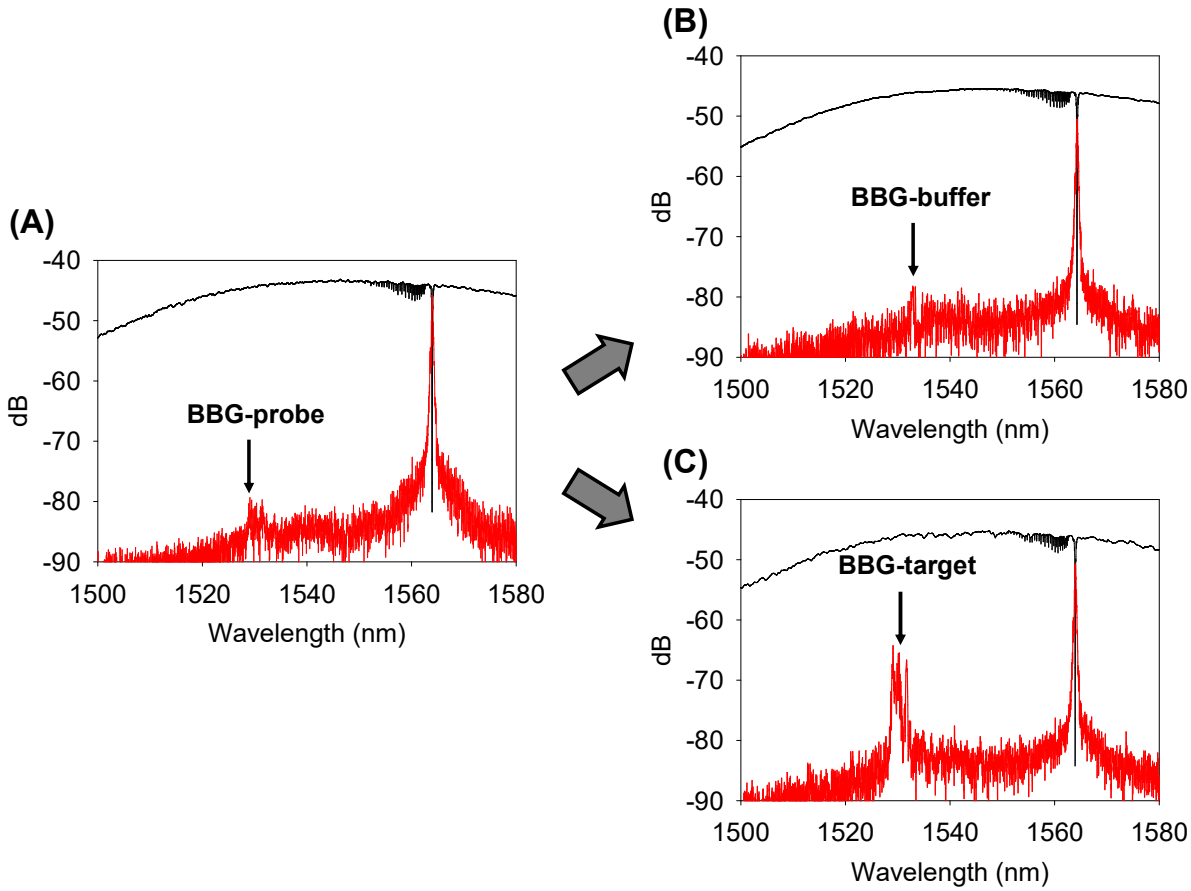

Figure S10. Reflection spectra obtained **(A)** after patterning BSA protein, **(B)** after incubating PBS-T buffer on them, and **(C)** after incubating a solution of 1 µg·mL^{-1} antiBSA in PBS-T**.** The reflectivity increase after incubating PBS-T is negligible, whereas a 20 dB increase (x100) is reached after incubating the antiBSA solution. Consequently, these results demonstrate that the increase of the reflection peak is due to biorecognition events. The transmission spectra indicate that some broadband loss (< 1 dB) is induced during the biorecognition process, which must come from some optical scattering due to the immersion of the microfibers in the solutions. To separate this effect from the biorecognition events, the reflectivity of the BBG was referenced to that of the FBG.

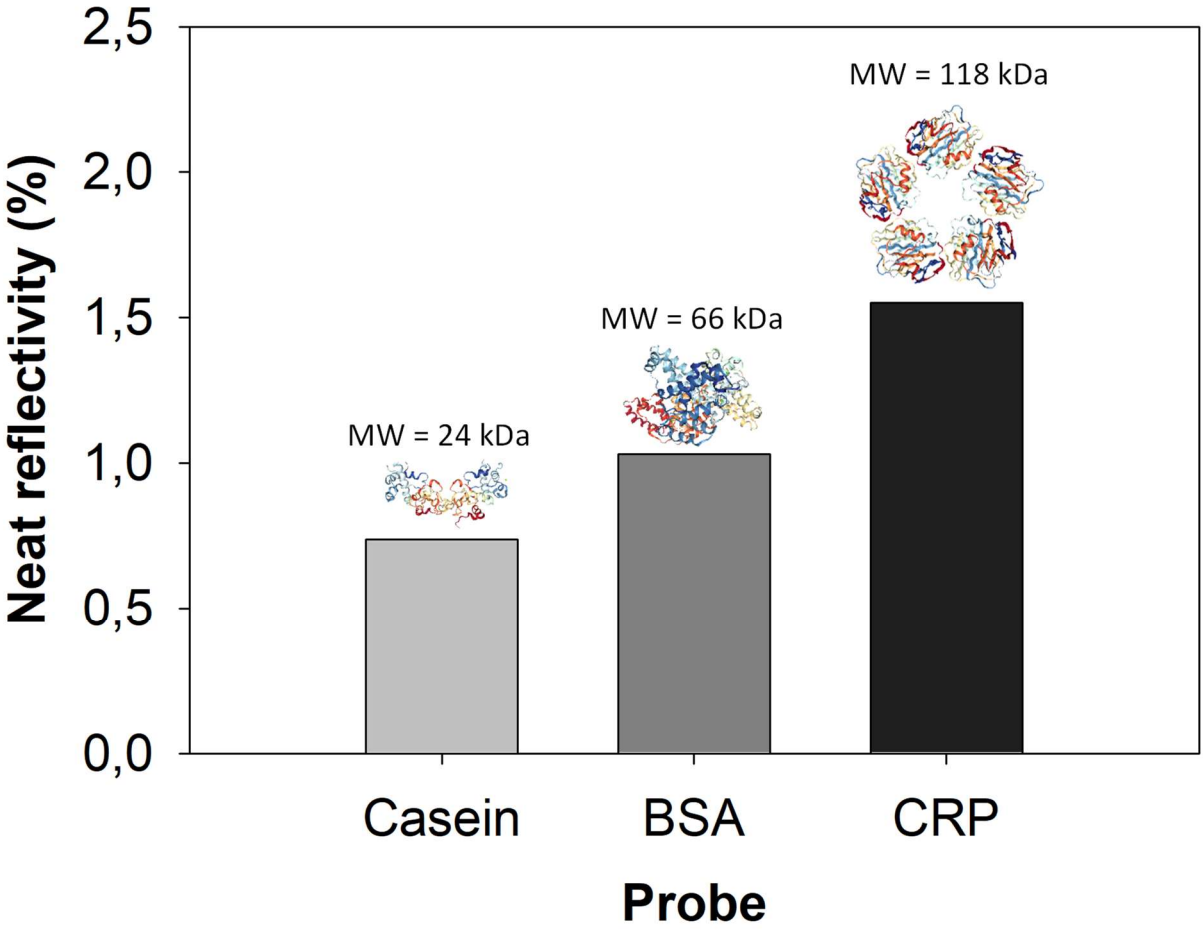

Figure S11. Peak reflectivities registered for BBGs of casein, BSA and CRP patterned on different microfibers.